# Coercivity in Exchange-Bias Bilayers

M. D. Stiles and R. D. McMichael

*National Institute of Standards and Technology, Gaithersburg, MD 20899*

(November 3, 2000)

## Abstract

A model is presented for coercivity in polycrystalline exchange-bias bilayers. It includes two contributions for their enhanced coercivity, inhomogeneous reversal and irreversible transitions in the antiferromagnetic grains. The model can be characterized in terms of a small number of dimensionless parameters, and its behavior has been determined through simulations of magnetic reversal for a range of values of these parameters. In these simulations, the first contribution to the coercivity arises from energy losses in the ferromagnet due to irreversible transitions over small, local energy barriers in the ferromagnetic film due to the inhomogeneous coupling to the antiferromagnet. This inhomogeneous reversal contributes to the coercivity at all temperatures. The second contribution to the coercivity arises from energy losses in the antiferromagnet due to irreversible transitions of the antiferromagnetic order in the grains. In the present model, the antiferromagnetic order only becomes unstable at non-zero temperature, so that this contribution to the coercivity only occurs at non-zero temperatures. In addition to the coercivity, the computed hysteresis loops are found to be asymmetric, and the loop shift is shown to differ from the grain-averaged unidirectional anisotropy.

## I. INTRODUCTION

An exchange-bias bilayer consists of a ferromagnetic thin film coupled to an antiferromagnetic film. The most commonly observed changes in the properties of the ferromagnetic thin film as a result of this coupling are a shift in its hysteresis loop and an increase its coercivity, or width of its hysteresis loop.[1,2] Several models[3–6] can explain the size of the loop shift, but the increase in the coercivity is less well understood.

There are several possible mechanisms which have been used to explain the increased coercivity found in exchange bias systems. One mechanism for coercivity in these systems derives from instabilities in the antiferromagnet.[3,7,8] If reversing the ferromagnetic magnetization irreversibly switches the antiferromagnetic order in parts of the system, work is done. This work must contribute to the area and hence width of the hysteresis loop. Another mechanism for coercivity is inhomogeneous magnetization reversal. If the sample has inhomogeneous properties, these can lead to a coercivity through mechanisms like domain-wall pinning.[9,10] We consider both these mechanisms in this paper.

The most commonly invoked mechanism for coercivity is reversal through coherent rotation. In coherent rotation, the ferromagnetic magnetization is assumed to be spatially uniform during reversal. The presence of an anisotropy in the ferromagnetic film gives barriers to rotation that are irreversibly overcome during reversal. Since this model has only one degree of freedom, the direction of the ferromagnetic magnetization, it is frequently used to fit experimental results. In several theoretical models,[11,12] perpendicular coupling[13] at the interface gives the ferromagnet the effective uniaxial anisotropy that causes the coercivity.

There are several arguments against coherent rotation with a uniaxial anisotropy as the origin of the enhanced coercivity in these systems. One argument is based on the measurement of hysteresis in samples prepared with ferromagnetic layer that continuously increases in thickness, i.e. a wedge-shaped ferromagnetic layer.[14,15] Since the loop shift is found to vary as the inverse of the ferromagnetic layer thickness, different parts of the sample reverse at different applied fields. Thus, between the reversed and unreversed parts

of the sample, there is a domain wall that moves across the sample as the field is varied. If the sample were spatially uniform, as is assumed for coherent rotation, the domain wall would be free to move to its minimum energy site. In this case, the domain wall would sit exactly at the place on the film where the shift field is equal to the external field. It would pass through the same point at the same field for both directions of the field sweep and there would be no coercivity. However, measurements show that the coercivity is locally the same at each thickness as it is in uniform films of the same thickness that do not have a pre-existing domain wall. Thus, the coercivity cannot be simply due to a uniform uniaxial anisotropy and coherent rotation.

This conclusion is not restricted to these wedge samples. There is experimental evidence for the presence of domain walls in many exchange-bias systems. Images obtained by magnetic force microscopy,[16,17] magneto-optical indicator film imaging,[18,19] and Fresnel imaging[20] show the presence of domains and domain walls during reversal. Furthermore, images of 360° domain walls in exchange-biased films[21] are evidence that the magnetization rotates in different directions in different parts of the film.

It is also possible to test whether the uniaxial anisotropy is the origin of the coercivity by measuring the anisotropy directly in experiments like ferromagnetic resonance,[22–24] Brillouin light scattering,[25,26] and rotational torque.[27–31] The uniaxial anisotropy that is measured in these systems is frequently not large enough to account for the measured coercivity.

In this paper, we compute the loop shift and coercivity for an extension of a model[32,33] that we previously used to describe measurements in a saturating field, like ferromagnetic resonance and rotational torque. This model includes both instabilities in the antiferromagnet and inhomogeneities as mechanisms for increased coercivity. In Sec. II we briefly describe the model and its extensions. In Sec. III we give the results of our calculations.

## II. MODEL

In previous papers,[32,33] we describe a model for polycrystalline exchange-bias systems, and calculate properties of the systems in applied magnetic fields that are large enough to saturate the ferromagnetic magnetization. A brief summary of the model follows. In this model, we assume that the grains of the antiferromagnet are independent (not coupled to each other), and each is coupled only to the ferromagnetic layer. Each antiferromagnetic grain has uniaxial anisotropy with easy-axis directions randomly distributed in three dimensions (uniformly distributed over the surface of a sphere). The coupling between the antiferromagnetic grains and the ferromagnetic film is assumed to be distributed according to a statistical distribution of the fraction of each sublattice at the interface. The net interfacial coupling varies from grain to grain due to the statistical distribution of the two sublattices at the interface of each grain. The mean interfacial coupling is the average over all grains of the absolute value of the strength of the coupling. We do not include any perpendicular or spin-flop coupling.

In this model, the zero-temperature properties are described by two parameters, the domain-wall energy in the antiferromagnet, $\sigma_0$, and the dimensionless ratio of the mean interfacial coupling to the domain wall energy

$$r_0 = \frac{2J_{\rm int}}{\sigma_0 a^2}\sqrt{\frac{2}{\pi N}}, \tag{1}$$

where $J_{\rm int}$ is the bare coupling across the interface, $N$ is the number of spins at the interface of each grain, and $Na^2$ is the interface area of the grains. See Table I for the definitions of all the dimensionless parameters used in this model.

There are two sources of temperature dependence in the model. First, we assume that the domain-wall energy in the antiferromagnet depends on temperature as $\sigma = \sigma_0(1-T/T_{\rm N})^{5/6}$, where $T_{\rm N}$ is the Néel temperature. Second, we assume that the finite-size antiferromagnetic grains behave analogously to superparamagnets as assumed earlier by Fulcomer and Charap.[7] These authors treated a model in which the barrier to reversal is determined by

a volume anisotropy. We assume that it is determined by a domain-wall energy. For very small grains, the former is likely to be a good approximation, and for larger grains where the reversal mechanism is non-uniform the latter will be a better approximation. None of the results we discuss below depend qualitatively on which model for reversal is chosen.

We assume that each antiferromagnetic grain exists in one of two states. Far from the interface with the ferromagnet, the states differ only in the direction of the sublattice magnetizations along the easy axis. In the absence of coupling to the ferromagnet, the two states are degenerate, but the coupling to the ferromagnet winds up partial domain walls[3,32,34,35] in the antiferromagnet and lifts the degeneracy. As a function of the ferromagnetic magnetization direction, $\hat{\mathbf{M}}_{\mathrm{FM}}$, the energies of the two states are

$$E^{(\pm)} = \frac{Na^2\sigma}{2}\left(1 - \left[1 + 2r\hat{\mathbf{M}}_{\mathrm{FM}} \cdot (\pm\hat{\mathbf{u}}) + r^2\right]^{1/2}\right), \tag{2}$$

where $\hat{\mathbf{u}}$ is the easy axis in the antiferromagnet grain, and $r$ is the ratio of the net interfacial coupling for that grain to the domain-wall energy times the area of the grain. We assume that the energy barrier from the state that is higher in energy to the state that is lower in energy is given by the change in energy plus a domain-wall energy times the interface area of the grain. The barrier for the transition from the low state to the high state is just a domain wall energy times the area.[36]

With this model for the barriers between the two configurations, the two parameters that determine the temperature dependence in this model are the Néel temperature, $T_{\mathrm{N}}$ and the dimensionless ratio of the zero-temperature domain-wall energy to the Néel temperature

$$b = \frac{Na^2\sigma_0}{kT_{\mathrm{N}}}. \tag{3}$$

This parameter characterizes the ratio of the typical size of the reversal barriers to typical thermal energies.

For properties of the system when the ferromagnetic magnetization is saturated, as treated in previous papers,[32,33] the parameters described above are the only parameters of the model. However, in the present paper, in which we are interested in non-uniform

magnetization reversal, both the spatial distribution of the grains and the exchange stiffness in the ferromagnetic film matter. For simplicity we assume that the antiferromagnetic grains are uniformly spaced on a square grid. We also assume that the magnetization in the ferromagnetic film is uniform throughout the thickness of the film. By definition, this assumption is correct when the ferromagnetic magnetization is saturated. Neutron scattering[37] shows that it is correct more generally, at least for some samples. On the other hand, this assumption is likely to be inappropriate for systems like $Fe/FeF_2$[38–40], in which it appears that domain walls parallel to the interface do play an important role.[41]

The new parameter of the model, necessary to compute coercivity, describes the extent to which inhomogeneities are important. It is defined in terms of averaged quantities as the ratio of the strength of the coupling at the interface to the intergranular coupling in the ferromagnetic film

$$s = \frac{Na^2\sigma_{\rm ex}(0)}{At}, \tag{4}$$

where $A$ is the exchange stiffness constant in the ferromagnet, $t$ is the thickness of the ferromagnet, and $\sigma_{\rm ex}(0)$ is the size of the unidirectional anisotropy at $T = 0$. From earlier work,[32,33] the zero-temperature unidirectional anisotropy is given by

$$\sigma_{\rm ex}(0) = \frac{\sigma_0}{2}\int_0^\infty dr\Phi(r, r_0)F_1(r), \tag{5}$$

where

$$F_1(r) = \begin{cases} \frac{r}{2}\left(1 - \frac{r^2}{5}\right) & r < 1 \\ \frac{1}{2}\left(1 - \frac{1}{5r^2}\right) & r > 1 \end{cases}, \tag{6}$$

and

$$\Phi(r, r_0) = \frac{2}{\pi r_0}\exp\left(-\frac{r^2}{\pi {r_0}^2}\right), \tag{7}$$

is the distribution of interfacial coupling energies.

We compute hysteresis loops for this model by integrating the damped equations of motion for the ferromagnetic layer. The equations are derived from equations of motion in the

Landau-Lifshitz form by dropping the precessional term. Then, we restrict the ferromagnetic magnetization to lie in the plane. Finally, we ignore the thermal noise associated with the damping through the fluctuation-dissipation theorem. While these approximations give rise to additional uncertainly in the results, we believe the resulting changes are minor, the approximations allow us to focus on effects intrinsic to the coupling to the antiferromagnet, and they significantly speed up the calculation, allowing the systematic exploration of phase space given below. Using this procedure, the time scale of damped motion can be determined from the dimensionless damping parameter $\alpha$ and the gyromagnetic ratio, $g$. The damped equation of motion is then

$$\dot{\phi}_{i,j} = -\lambda' \frac{\partial \varepsilon'_{i,j}}{\partial \phi_{i,j}}, \tag{8}$$

where

$$\begin{aligned} \varepsilon_{i,j} = & -\frac{1}{2} \sum_{i',j' \in \text{n.n.}} \cos(\phi_{i,j} - \phi_{i',j'}) \\ & - \frac{\mu_0 M_{\text{S}} H N a^2}{A} \cos(\phi_{i,j} - \phi_{\text{H}}) \\ & - \frac{\sigma N a^2}{2At} \sqrt{1 \pm 2 r_{i,j} \sin\theta_{i,j} \cos(\phi_{i,j} - \psi_{i,j}) + r_{i,j}^2} \end{aligned} \tag{9}$$

is the dimensionless energy (scaled by $At$) associated with the ferromagnetic grain of volume $Na^2t$ located at site $(i, j)$. The first term is the exchange coupling with nearest-neighbor sites, the second term is the interaction with the external field, and the last term is the coupling to the antiferromagnetic grain at that site. The orientation of the easy axis in the antiferromagnetic grain is described by the polar angle $\theta_{i,j}$ and the azimuthal angle $\psi_{i,j}$. The interfacial coupling compared to the domain-wall energy is given by $r_{i,j}$. The coupling energy depends on the state of the antiferromagnet, through the $\pm$ sign. The time scale is determined by the rate

$$\lambda' = \frac{A}{Na^2} \frac{\alpha}{1+\alpha^2} \frac{g\mu_{\text{B}}}{\hbar M_s} \approx 1.5 \times 10^8 \text{ s}^{-1}, \tag{10}$$

based on the values

$$
\begin{aligned}
A &= 1.3 \times 10^{-11}\ \mathrm{J/m} \\
Na^2 &= 4 \times 10^{-16}\ \mathrm{m}^2 \\
\alpha &= 0.02 \\
g &= 2 \\
M_s &= 8 \times 10^5\ \mathrm{A/m}, \qquad (11)
\end{aligned}
$$

which are representative values of materials parameters for $Ni_{80}Fe_{20}$.

In Section III, we compute hysteresis loops in two different ways. At zero temperature, since there are no thermally activated processes, it is possible to define a meaningful quasi-static limit. For zero-temperature computations, we use a combination of conjugate-gradient minimization and direct integration of the damped equation of motion to compute the quasi-static hysteresis loops. The field is varied in small discrete steps. For each new field, we use conjugate-gradient minimization to minimize the energy of the configuration. If the change in configuration is large enough, indicating that some part of the system has changed discontinuously, we redo the energy minimization using direct integration of Eq. (8). This last step ensures that the system does not go over any energy barriers inappropriately due to an overly large step in the conjugate gradient procedure. For both simplicity in the model and computational speed, we ignore the contribution of the precessional motion to overcoming energy barriers.

At finite temperature, we allow for thermal transitions between the two states of each of the antiferromagnetic grains. As described previously,[33] for a given configuration of the system, our model gives a barrier, $E^{\mathrm{B}}_{i,j}$ for reversal for each of the antiferromagnetic grains. Together with the prefactor $\nu$, the barrier height and the temperature $T$ give a time scale for thermal excitation over the barriers. Since the thermal transitions in the antiferromagnetic grains and the equation of motion of the ferromagnet, Eq. (8), each have a definite time scale, it is straightforward to combine them. We vary the field in discrete steps as before, but directly integrate Eq. (8) for a fixed-number of time steps with fixed length, $\Delta t$. After each time step, we allow for thermal transitions between states in the antiferromagnetic grains.

For each grain, we compute the probability that the grain has made a transition over the barrier during the preceding time step

$$P_{ij}^{\mathrm{trans}}(\Delta t) = 1 - \exp\left[-\nu \Delta t \exp\left(-E_{ij}^{\mathrm{B}}/k\mathrm{B}T\right)\right]. \tag{12}$$

We accept the transition when the probability is larger than a random number chosen between zero and one. When the probability of a transition becomes appreciable, multiple transitions between the two antiferromagnetic states become possible in each time interval. In this case, the expression for the transition probability is modified so that the net probability distribution of the two states tends to its equilibrium value.

For finite-temperature calculations, the time scales of these transitions set a time scale for the hysteresis loop, and the quasi-static limit cannot be achieved. The hysteresis loops have a definite field sweep rate associated with them. For sufficiently slow sweep rates, the hysteresis loop changes very slowly with sweep rate.

## III. RESULTS

The model described in Sec. II contains two mechanisms that give coercivity. The first, which contributes at all temperatures, is due to inhomogeneities in the system. For this mechanism, the energy losses come from irreversible processes in the ferromagnetic film. The second, which contributes only at non-zero temperatures (in this model, all energy barriers are greater than zero), is due to irreversible processes in the antiferromagnetic grains. This mechanism for coercivity has been described previously.[7,8] However, the contribution to the coercivity from this mechanism is significantly reduced in the presence of inhomogeneities as is discussed below.

### A. Zero-temperature results

We illustrate the inhomogeneous mechanism for coercivity with a particular realization of the model described in the previous section. The system consists of a $16 \times 16$ lattice

with periodic boundary conditions. The biased state is prepared by choosing the state of each antiferromagnetic grain with the lowest energy when the field is pointed in the positive $x$ direction. The variation of the easy-axis directions in the randomly oriented antiferromagnetic grains gives rise to the inhomogeneity in this system. This inhomogeneity is the only source of coercivity in this system. There is no anisotropy in the ferromagnetic grains except the effective anisotropy induced by the coupling to the antiferromagnet. If the ferromagnetic magnetization is constrained to be uniform over all the whole film, the only effective anisotropy is unidirectional. There is no macroscopic uniaxial anisotropy to give a barrier to reversal. In addition, there is no irreversibility in the antiferromagnetic grains at zero temperature in this model, so there is no contribution to the coercivity from such irreversibility.

Figure 1 shows the hysteresis loop calculated for this particular realization. Also illustrated are the spin configurations of the ferromagnetic grains at four points along the hysteresis loop. At high fields, the spins are all pointed in the positive $x$-direction. As the field is reduced, the antiferromagnetic grains exert torques on the moments of the ferromagnetic grains, rotating the spins toward the positive or negative $y$-direction, depending on the local easy-axis orientation. This rotation is illustrated in Panel (a). Grains that rotate toward the negative $y$-direction are shaded in gray, other grains rotate toward the positive $y$-direction. The intergranular exchange coupling between the ferromagnetic grains is strong enough that the moments must all rotate in the same direction on reversal. For the system illustrated here, the moments all rotate counterclockwise through the positive $y$-direction when going from positive fields to negative fields, as seen in Panel (b). Thus, the spins that started rotating in the negative $y$-direction see a local barrier to reversal. As the field is increased in the negative direction, the height of the barrier eventually goes to zero. When it does, the local moments rotate suddenly through some finite angle and dissipate energy. This energy loss is the origin of the hysteresis. It can be seen in the discrete jumps in the hysteresis loop.

At large negative fields, seen in Panel (c), the spin configuration is very closely related

to that in large positive fields, as seen in Panel (a). The moments are now are mostly in the negative $x$ direction, but the $y$-components are not reversed. It will be important below that for reversal in increasing, Panel (b), and decreasing fields, Panel (d), the rotation of the moments has the opposite sense. For this realization, the moments rotate through the positive $y$-direction in both cases.

In the hysteresis loop in Fig. 1, the magnetization and fields are given in terms of scaled variables. The magnetization is scaled by the saturation magnetization, and the field in terms of the shift field expected from the zero temperature unidirectional anisotropy,

$$\begin{aligned} m &= \frac{M}{M_{\rm S}} \\ h &= \frac{H\mu_0 M_{\rm S} t}{\sigma_{\rm ex}(0)}. \end{aligned} \tag{13}$$

Figure 1 illustrates that the loop shift can be different than what would be expected simply from the unidirectional anisotropy and that the loop is generally asymmetric. If the unidirectional anisotropy were uniform, it would behave like an applied field. When the hysteresis loop is measured along the easy direction of this anisotropy, the loop is symmetric around the shift field, $h = -1$. However, when the unidirectional anisotropy is not uniform, as it is not in this model, the reversal process will be different for the two directions and the shift field will be different than what would be expected from the effective unidirectional anisotropy.

Non-uniform reversal and coherent rotation lead to different behavior. This difference in illustrated in Fig. 2, which shows the angular dependence of the shift field and the coercive field as a function of the angle at which the external field is applied relative to the easy direction of the unidirectional anisotropy. Here, the systems are $128\times128$ lattices, still at zero temperature. Panel (a) gives the results for coherent rotation with a uniaxial anisotropy, and Panels (b) and (c) give results for realizations of the present model for two different sets of parameters. The angular dependence is not very different from what is found for the coherent rotation model. For the same ratio of the coercivity to loop shift at $\phi_{\rm H} = 0$, some choices of parameters give non-zero coercivity over a greater angular range than is found

for coherent rotation, but the difference can be subtle. For both coherent rotation and non-uniform reversal, the angular variation is consistent with the experimental results of Xi and White.[42] However, as seen in the insets to each panel, the two models give hysteresis loops that are very different for fields applied along the easy direction. For coherent rotation, the whole system changes discontinuously from one orientation to the other at a single field, giving a square hysteresis loop. For non-uniform reversal, the reversal consists of some parts reversible rotation and other parts small jumps over a limited part of the sample. To get a finite width hysteresis loop, there must be jumps with their associated irreversibility. For non-uniform reversal, these jump occur in small parts of the system giving a rounded appearing hysteresis loop. This loop shape is consistent with that found in the experiment mentioned above.[42]

In panels (b) and (c) of Fig. 2, the system was prepared in its maximally biased state, so that all the antiferromagnetic grains contribute to the bias. In panel (e), the antiferromagnetic grains are ordered completely randomly. In this model, there is no loop shift, but there is a constant coercivity for all field angles, $\phi_{\rm H}$. This coercivity is approximately the same as the easy direction coercivity for the completely biased sample. This similarity implies that the bias is responsible for eliminating the coercivity at other angles. Apparently, the bias gives a preferred direction for the rotation from one saturated state to the other, and causes the rotation to be reversible, eliminating the coercivity. In panel (d), half of the grains contribute to the bias and the other half are randomly ordered. For this model, the coercivity does not go to zero away from the easy direction, but exhibits behavior very similar to that found by Ambrose et al.[43]

The dependence of the coercivity and loop shift on the strength of the intergranular coupling is shown in Fig. 3. For the range of parameters considered here, both the scaled coercive field and loop shift appear to depend linearly on the ratio $s$, defined in Eq. (4), of interfacial coupling to intergranular coupling. For each value of $s$, completely different realizations of the 128×128 lattice were chosen. For two points, a set of 20 calculations were done giving an estimate of the variation from realization to realization. The deviation

of the calculated curves around linear behavior is apparently due to fluctuations from realization to realization. Much smoother curves would result if the parameters describing the antiferromagnetic grains were kept fixed as $s$ was varied.

The simplest way to vary the intergranular coupling experimentally is to vary the thickness of the ferromagnetic overlayer. The parameter $s$ depends inversely on the thickness. However, the scaling parameter for the field, Eq. (13) also depends linearly on the thickness. Thus the inverse dependence of the coercivity shown in Fig. 3 translates into an unscaled coercive field that decreases as one over the thickness squared, as shown in Fig. 4. This behavior is in contrast to the $t_{\rm FM}^{-3/2}$ behavior found in related calculations for a slightly different model.[9,10] The present model also predicts that the loop shift does not vary simply as inversely proportional to the thickness, but that there is a small correction that is proportional to one over the thickness squared.

The coefficients of linear variations shown in Fig. 3 depend weakly and non-monotonically on the other system parameter $r_0$. For a given strength of coupling at the interface, i.e. $\sigma_{\rm ex}(0)$ constant, varying $r_0$ effects the system in two ways. First, it affects the distribution of $r$ values. When $r_0$ is much less than one, $\Phi(r, r_0)$, contains only small values of $r$. For small $r$ the amplitude of the angular variation in Eq. (2) is proportional to $r$, so that the distribution of coupling strengths is relatively broad. On the other hand, when $r_0$ is much greater than one, $\Phi(r, r_0)$ contains predominantly large values of $r$. For large $r$ the amplitude of the angular variation in Eq. (2) is independent of $r$, so that the distribution of coupling strengths is relatively narrow. Second, $r_0$ affects the presence of higher harmonics in the coupling at the interface. When $r$ is either much smaller than one or much larger than one, the angular dependence of the interfacial energy, Eq. (2), varies simply as the cosine of the angle between the ferromagnetic magnetization direction and the easy axis. However, when $r$ is close to one, there are higher odd harmonics. The presence of these harmonics increases the asymmetry between the hard and easy directions.

Figure 5 shows the convergence of the simulations with respect to size. There are two issues. First, the system must be large enough that the periodic boundary conditions do not

affect the results. The bottom panel of Fig. 5 shows that $32 \times 32$ and $64 \times 64$ lattices show such size dependences, but the $128 \times 128$ lattices do not. The second issue is whether the lattice is large enough to give an average value with one simulation. The top panel of Fig. 5 shows that the $128 \times 128$ lattices are not quite large enough. The variations from realization to realization give the uncertainties shown in Fig. 3. The simulations described in Fig. 3 use $128 \times 128$ lattices, which are not quite large enough to be converged with respect to lattice size. However, they were the largest size that was practical.

In the current model, each antiferromagnetic grain has a local unidirectional anisotropy. The local unidirectional anisotropies, Eq. (2), have a distribution determined by the distribution of $r$ values in Eq. (7) and the distribution of polar angles of the easy axis directions. The resulting distribution has a large narrow peak around zero, but there is a long tail extending to relatively large values. A large lattice is required to sample the tails of the distribution accurately. If the distribution were more uniform, smaller lattices would be adequate. For example, if the value if $r$ is fixed and not distributed, then $64 \times 64$ lattices are adequate. Alternatively, models in which the easy axis directions are restricted to be in-plane would require smaller lattices.[10]

### B. Finite temperature results

For simulations at finite temperature the rate at which the magnetic field is changed becomes important. If it were feasible to reverse the magnetization slowly enough that the system were in equilibrium the whole time, there would be no hysteresis. However, the time scale for this is unrealistically long in all but trivial cases. When there is a loop shift, some of the antiferromagnetic grains are stable on the time scale of the measurement. Which grains are stable depends on the time scale of the measurement and the temperature. The variation of the temperature dependence as a function of sweep rate is illustrated in Fig. 6.

Using the parameters chosen in Eq. (10), the simulations illustrated in Fig. 6 are done by varying the magnetic field between 48000 A/m (600 Oe) and -48000 A/m in $2 \times 10^{-4}$ s

to $16 \times 10^{-4}$ s. Ideally, slower sweep rates would be desirable, but were not feasible. The simulation with the slowest sweep rate integrated $2.4 \times 10^6$ time steps for each of $128 \times 128$ spins at each of ten temperatures. At low temperatures, the coercivity depends strongly on the sweep rate. At zero temperature, where it is possible to compute a quasi-static limit, the constant sweep-rate results approach, but do not reach, the quasi-static limit. The loop shift does not depend strongly on the sweep rate except that the blocking temperature increases slowly as the sweep rate is increased.

In Ref. 33, we computed the unidirectional anisotropy as a function of temperature assuming a measurement time of 0.5 s. With the sweep rates considered here, a much shorter measurement time is appropriate. In Fig. 7, we compare the loop shifts computed from simulations as described above using sweep rates of $4 \times 10^{-4}$ s to calculations like those in Ref. 33 based on a measurement time of $10^{-3}$ s, which is approximately the time required for a full hysteresis loop in the simulation. At low temperatures, the loop shift found in these simulations is always lower than the loop shift that would be expected from the unidirectional anisotropy. However, at higher temperatures the curves can cross and the loop shifts become greater than the values expected from the averaged unidirectional anisotropy. While this could be due to a shift in the blocking temperature resulting from different effective measuring times, the difference clearly indicates that loop shifts and macroscopic unidirectional anisotropies need not be the same. This becomes particularly true if the effective measurement times are very different for the two measurements.

At low temperatures, the coercivity found in these simulations tracks the zero temperature results over a range of parameter values, as seen in Fig. 8. For larger values of $r_0$, the coercivity is temperature dependent down to $T = 0$. This result follows simply from the fact that for these values of $r_0$, the coupling between the antiferromagnet and the ferromagnet is limited by the domain wall energy in the antiferromagnet, and that energy is temperature dependent. At higher temperatures, there is a peak in the coercivity that is associated with instabilities in the antiferromagnetic grains. The double peak structure seen particularly for $r_0 = 1.0$ and $b = 300$ is reminiscent of the behavior found by Gökemeijer and Chien.[44]

The processes that give rise to high-field rotational hysteresis measured in rotational torque experiments are related to the losses in a hysteresis loop measurement. In Fig. 8, we compare the coercivities found in these simulations with those expected based on calculated rotational hysteresis results as in Ref. 33, but with the measurement time of $10^{-3}$ s. At temperatures just below the blocking temperature there are clearly contributions from the coercivity that are due to hysteretic losses in the antiferromagnet. There are peak values that are significantly greater than the value of the coercivity found at $T = 0$ due to inhomogeneous reversal. However, as the temperature is further decreased, the coercivity decreases much more quickly than the rotational hysteresis.

The difference between coercivity and rotational hysteresis can be understood in terms of the critical angles as in Fig. 7 of Ref. 32 and Fig. 1 of Ref. 33. In a rotational torque measurement, all grains go through at least one and usually two critical angles at which the state switches to the other energy curve. In Ref. 33, it was assumed that all grains had two such transitions. However, as discussed with respect to Fig. 1, the magnetization does not rotate through 360° during a hysteresis loop measurement. It rotates through 180° and then −180° on the reverse field sweep. Thus, there are many grains that will never go through a critical angle *for the configuration they are in* during a hysteresis loop measurement. As the temperature is lowered, the critical angles become larger and larger, and fewer and fewer grains make hysteretic transitions that contribute to the coercivity, but they still contribute to the rotational hysteresis.

In addition to the high-field rotational hysteresis, there are other experimental manifestations of instabilities in the antiferromagnet in exchange-bias systems. One of these is an isotropic field shift found in ferromagnetic resonance measurements.[23] This field shift can be explained in terms of a rotatable anisotropy, an effective anisotropy that is fixed on the precessional time scale, but which rotates on the much longer time scale on which the external field is rotated.

Interestingly, the coercivity seems to track the rotatable anisotropy better than the rotational hysteresis. We do not have a good explanation for this result. At low temperatures,

when the antiferromagnetic grains behave reversibly, each grain contributes a unidirectional anisotropy, which is distributed in both orientation and strength. At high temperatures, where the antiferromagnetic grains switch between both states, each grain provides a local uniaxial anisotropy to the antiferromagnet. The rotatable anisotropy is an indirect measure of the local variations in this uniaxial anisotropy. However, test simulations using a reasonable distributions of such uniaxial anisotropies give coercivities much smaller than those found with the full model. Perhaps including higher harmonics in the anisotropy would improve the picture, but we believe that the losses in the antiferromagnetic grains play an important role in this regime, and these losses are not captured in a model with local uniaxial anisotropies.

Figure 9 shows how the loop shift and coercivity depend on the ratio of coupling $s$ between the ferromagnet and the antiferromagnetic grains to the intergranular coupling. This ratio has a big effect on the low-temperature coercivity, as it did in the zero-temperature simulations, but, at higher temperatures, the effect appears to be quite small for all of the simulations we have done. This behavior suggests that the contribution to the coercivity from the inhomogeneity is dependent on this ratio, but the contribution due to instabilities in the antiferromagnet is not. Since the ferromagnetic magnetization goes from saturation to saturation, the antiferromagnetic grain gets twisted through the same angle independent of the ratio of the coupling, and hence undergoes the same irreversible transitions. However at low temperature, when the losses occur in the ferromagnet more than the antiferromagnet, the coercivity depends strongly on this ratio.

The difference in behavior at high and low temperatures gives different thickness dependences at high and low temperatures as shown in Fig. 10. At zero temperature, in the quasi-static limit, the coercivity decrease like $t_{\mathrm{FM}}^{-2}$. In the finite-sweep-rate simulations, this behavior is obscured at large thicknesses by an increasing dependence of the coercivity on the sweep rate. At higher temperatures, in the regime where the losses are predominately in the antiferromagnet, the coercivity decreases like $t_{\mathrm{FM}}^{-1}$.

## IV. SUMMARY

In this paper we have simulated magnetic reversal in polycrystalline exchange-bias bilayers as would be measured in an hysteresis loop. We use a model we have previously applied to measurements made in saturated magnetic states.[32,33] These simulations exhibit two contributions to the enhanced coercivity found in exchange-bias systems, one due to inhomogeneous reversal and the other to irreversible transitions in the antiferromagnetic grains.

The ferromagnetic thin film is coupled to an inhomogeneous environment due to the assumed random orientations of the easy axes of the antiferromagnetic grains. As the applied magnetic field is reduced from a large value and the ferromagnet relaxes from its saturated state, parts of the magnetization are twisted one way and parts the other. When the ferromagnet ultimately reverses, much larger areas will rotate in the same direction. Thus there are a large number of local barriers to reversal. As each of them is overcome, there is energy lost in the ferromagnetic film. Because there are a lot of small barriers that are sequentially overcome, the hysteresis loop becomes rounded. This reversal mechanism is strongly dependent on the ratio of the coupling between the ferromagnetic film and the antiferromagnetic grains to the intergranular exchange coupling in the ferromagnetic film. As the coupling within the ferromagnetic film becomes stronger, the relative twisting in the ferromagnetic film becomes smaller, and the coercivity decreases. This decrease leads to a thickness dependence, $H_{\rm c} \propto t_{\rm FM}^{-2}$. The loop shift is generally smaller than expected from the macroscopic unidirectional anisotropy. It decreases linearly with the film thickness, but has a small quadratic correction.

At higher temperatures, the coercivity becomes dominated by hysteretic losses occurring in the antiferromagnetic grains. As the ferromagnetic magnetization is rotated, the state of the antiferromagnetic grain can become unstable and switch. This irreversible switching leads to loss and the associated coercivity. It is closely related to the losses that give rise to the high-field rotational hysteresis that is observed in these systems. However, as

the temperature decreases, the contribution of these processes to coercivity becomes much smaller than their contribution to the rotational hysteresis. The difference arises because the magnetization rotates in opposite directions on the forward and reverse parts of the hysteresis loop measurement. In this regime, the coercivity does not depend strongly on the coupling within the ferromagnetic film, and so decreases with film thickness like $H_c \propto t_{FM}^{-1}$. Here the loop shift can be greater or less than expected from the macroscopic unidirectional anisotropy, as both depend on the details of the measurement, particularly its time scale.

# REFERENCES


[1] W. H. Meiklejohn and C. P. Bean, Phys. Rev. **102**, 1413 (1956).

[2] Two recent review articles are J. Nogués and I. K. Schuller, J. Magn. Magn. Mater. **192**, 203 (1999), and A. E. Berkowitz and K. Takano, J. Magn. Magn. Mater. **200**, 552 (1999).

[3] L. Néel, Ann. Phys. (Paris) **2**, 61 (1967). An English translation is available, in "Selected Works of Louis Néel," ed. N. Kurti, (Gordon and Breach Science Publishers, New York, 1988), p. 469.

[4] A. P. Malozemoff, Phys. Rev. B **35**, 3679 (1987); J. Appl. Phys. **63**, 3874 (1988).

[5] K. Takano, R. H. Kodama, A. E. Berkowitz, W. Cao, and G. Thomas, Phys. Rev. Lett. **79**, 1130 (1997).

[6] D. Mauri, H. C. Siegmann, P. S. Bagus, and E. Kay, J. Appl. Phys. **62**, 3047 (1987).

[7] E. Fulcomer and S. H. Charap, J. Appl. Phys. **43**, 4190 (1972).

[8] K. Nishioka, C. Hou, H. Fujiwara, and R. D. Metzger, J. Appl. Phys. **80**, 4528 (1996).

[9] S. Zhang, D. V. Dimitrov, G. C. Hadjipanayis, J. W. Cai, and C. L. Chien, J. Magn. Magn. Mater., **198-199**, 468 (1999).

[10] Z. Li and S. Zhang, Phys. Rev. B, **61** R14897 (2000).

[11] T. C. Schulthess and W. H. Butler, Phys. Rev. Lett. **81**, 4516 (1998).

[12] R. E. Camley, B. V. McGrath, R. J. Astalo, R. L. Stamps, J.-V. Kim, and L. Wee, J. Vac. Sci. Technol. A **17**, 1335 (1999).

[13] N. C. Koon, Phys. Rev. Lett. **78**, 4865 (1997).

[14] S. M. Zhou, K. Liu, and C. L. Chien, Phys. Rev. B **58**, R14717 (1998).

[15] V. I. Nikitenko, V. S. Gornakov, A. J. Shapiro, R. D. Shull, K. Liu, S. M. Zhou, and C. L. Chien, Phys. Rev. Lett. **84**, 765 (2000).

[16] X. Lin, J. G. Zhu and G. Wang, IEEE Trans. Mag. **33**, 3987 (1997).

[17] M. Cartier, S. Auffret, Y. Samson and B. Dieny, private communication (preprint).

[18] V. S. Gornakov, V. I. Nikitenko, L. H. Bennett, H. J. Brown, M. J. Donahue, W. F. Egelhoff, R. D. McMichael and A. J. Shapiro, J. Appl. Phys. **81** 5215 (1997).

[19] V. I. Nikitenko, V. S. Gornakov, L. M. Dedukh, Yu. P. Kabanov, A. F. Khapikov, A. J. Shapiro, R. D. Shull, A. Chaiken and R. P. Michel, Phys. Rev. B. **57**, R8111, (1998), V. I. Nikitenko, V. S. Gornakov, L. M. Dedukh, Yu. P. Kabanov, A. F. Khapikov, A. J. Shapiro, R. D. Shull, A. Chaiken and R. P. Michel, J. Appl. Phys. **83**, 6828, (1998).

[20] X. Portier, A. K. Pettiford-Long, S. Mao, A. M. Goodman, H. Laidler and K. O'Grady, IEEE Trans. Mag, **35** 3091 (1999).

[21] H. S. Cho, C. Hou, M. Sun and H. Fujiwara, J. Appl. Phys. **85** 5160 (1999), H. S. Cho and H. Fujiwara, IEEE Trans. Mag., **35**, 3868, (1999).

[22] P. Lubitz, J. J. Krebs, M. M. Miller, and S. Cheng, J. Appl. Phys., **83**, 6819 (1998).

[23] R. D. McMichael, M. D. Stiles, P. J. Chen, and W. F. Egelhoff, Jr., Phys. Rev. B **58**, 8605 (1998); R. D. McMichael, M. D. Stiles, P. J. Chen, and W. F. Egelhoff, Jr., J. Appl. Phys., **83**, 7037 (1998).

[24] M. Rubinstein, P. Lubitz, and S. Cheng, J. Magn. Magn. Mater. **210**, 329 (2000).

[25] A. Ercole, T. Fujimoto, M. Patel, C. Daboo, R. J. Hicken, and J. A. C. Bland, J. Magn. Magn. Mater. **156** 121 (1996).

[26] P. Miltényi, M. Gruyters, G. Güntherodt, J. Nogués, I. K. Schuller, Phys. Rev. B **59**, 3333 (1999).

[27] W. H. Meiklejohn, J. Appl. Phys. **33**, 1328 (1962).

[28] D. Paccard, C. Schlenker, O. Massenet, R. Montmory, and A. Yelon, Phys. Stat. Sol. **16**,

301 (1966).

[29] C. Schlenker, J. de Phys. Coll. **C 2**, 157 (1968).

[30] C.-H. Lai, H. Matsuyama, R. L. White, T. C. Anthony, And G. G. Bush, J. Appl. Phys. **79**, 6389 (1996).

[31] M. Tsunoda and M. Takahashi, J. Appl. Phys., **87**, 6415 (2000); M. Tsunoda, Y. Tsuchiya, T. Hashimoto, and M. Takahashi, J. Appl. Phys., **87**, 4375 (2000).

[32] M.D. Stiles, and R.D. McMichael, Phys. Rev. B **59**, 3722 (1999).

[33] M.D. Stiles, and R.D. McMichael, Phys. Rev. B **60**, 12950 (1999).

[34] H. Fujiwara and M. Sun, J. Appl. Phys. **85**, 4940 (1999).

[35] H. Xi and R. M. White, Phys. Rev. B **61**, 80 (2000).

[36] In 33, we consider just the reversal processes nucleated at the interface so that the barrier from the low-energy state to the high-energy state was a domain-wall energy plus the difference in energy. This is a higher barrier than that for reversal nucleated at the back of the grain, in which case the barrier is just a domain-wall energy. In practice, the difference between these two approximations only affects the rotatable anisotropy above the blocking temperature, and above that point the differences are less than 15 %.

[37] S. S. P. Parkin, V.R. Deline, R. O. Hilleke, and G. P. Felcher, Phys. Rev. B **42**, 10583 (1990).

[38] T.J. Moran, J. Nogués, D. Lederman, and Ivan K. Schuller, Appl. Phys. Lett. **72**, 617 (1998).

[39] C. Leighton, J. Nogués, B. J. Jönsson-Åkerman, and Ivan K. Schuller Phys. Lett. **84**, 3466 (2000).

[40] M. R. Fitzsimmons, P. Yashar, C. Leighton, Ivan K. Schuller, J. Nogués, C. F. Majkrzak,

and J. A. Dura Phys. Lett. **84**, 3986 (2000).

[41] M. Kiwi, J. Mejí-López, R. D. Portugal, and R. Ramírez, Europhys. Lett. **48**, 573 (1999).

[42] H. Xi and R. M. White, J. Appl. Phys. **86**, 5169 (1999).

[43] T. Ambrose, R. L. Sommer, and C. L. Chien, Phys. Rev. B **56**, 83 (1997).

[44] N. J. Gökemeijer and C. L. Chein, J. Appl. Phys. **85**, 5516 (1999).

## TABLES

| Parameter | Definition | Meaning |
|---|---|---|
| $r_0$ | $\frac{2J_{\rm int}}{\sigma_0 a^2}\sqrt{\frac{2}{\pi N}}$ | Mean interfacial coupling energy scaled by domain wall energy. |
| $b$ | $\frac{Na^2\sigma_0}{kT_{\rm N}}$ | Domain wall energy scaled by Néel temperature. |
| $s$ | $\frac{Na^2\sigma_{\rm ex}(0)}{At}$ | Unidirectional anisotropy scaled by intergranular exchange. |
| | $T/T_{\rm N}$ | Temperature scaled by Néel temperature. |
| $m$ | $\frac{M}{M_{\rm S}}$ | Magnetization scaled by saturation magnetization. |
| $h$ | $\frac{H\mu_0 M_{\rm S} t}{\sigma_{\rm ex}(0)}$ | Applied field scaled by unidirectional anisotropy. |

TABLE I. Dimensionless parameters and variables. The domain wall energy and the unidirectional anisotropy refer to the zero temperature values.

## FIGURES

FIG. 1. Spin configurations during reversal. Panels (a-d) show the direction of the ferromagnetic magnetization as seen from above. Each arrow is associated with a separate grain. Grains with magnetization tilted slightly in the negative $y$-direction are highlighted in gray. Each configuration is connected to the point where it occurred on the hysteresis loop, shown in terms of scaled variables, see Eq. (13). $h = -1$ is the loop shift expected from the size of the unidirectional anisotropy. To the left in the figure are two arrows giving the positive $x$- and $y$-directions.

FIG. 2. Angular dependence of coercivity and loop shift. Each panel shows the coercivity $h_{\rm c}$ and loop shift $h_{\rm s}$ as a function of the angle $\phi_{\rm H}$ at which the magnetic field is applied relative to the easy axis direction of the unidirectional anisotropy. The insets in each panel show the hysteresis loop at $\phi_{\rm H} = 0$; the $y$-axis is located at $h = 0$ in all cases. Panel (a) gives the results for coherent rotation with a uniaxial anisotropy. Panels (b-e) give results for the present model for different values of $r_0$ Eq. (1), and of the fraction $f$ of grains contributing to the biased state. All fields and magnetizations are scaled as in Eq. (13).

FIG. 3. Dependence of coercivity and loop shift on intergranular exchange coupling. The scaled field values, as in Eq. (13), are plotted against the ratio of the coupling to the antiferromagnet to the coupling to neighboring ferromagnetic grains, as in Eq. (4), for different values of the parameter $r_0$, Eq. (1). The points with error bars are the mean values of 20 different configurations for $r_0 = 1.0$. The error bars give the widths of the distributions of values, not the uncertainty in the mean value. That uncertainty is smaller by a factor of $\sqrt{19}$. Rather the error bars represent single standard deviation uncertainties for points on the curves. Each point on the curves has only been calculated once. Different configurations have been used for each point.

FIG. 4. Dependence of coercivity on thickness. Using the parameter values in Eq. (11) and the value of the antiferromagnetic domain wall energy $\sigma_0$=1.0 mJ/m$^2$, the results from Fig. 3 are converted into the coercive field as a function of the thickness of the ferromagnetic film. Changing the value of the antiferromagnetic domain wall energy simply translates the curves horizontally.

FIG. 5. Lattice-size convergence. The top panel shows the hysteresis loops calculated for 16 different configurations of $128 \times 128$ lattices. The bottom panel shows the average hysteresis loops for 4 $256 \times 256$ lattices, 16 $128 \times 128$ lattices, 64 $64 \times 64$ lattices, and 256 $32 \times 32$ lattices. Averages are over the same total number of spins in each case.

FIG. 6. Sweep-rate dependence. The scaled loop shift, $h_{\rm s}$ and coercivity $h_{\rm c}$ as a function of temperature are calculated for several different sweep rates. The curves are labeled by the sweep rate in $10^7$ $\mathrm{Am^{-1}s^{-1}}$ based of the values of parameters in Eq. (11). The arrows to the left of the $y$-axis give the values calculated at $T = 0$ in the quasi-static limit.

FIG. 7. Loop shift and unidirectional anisotropy. For different parameter values given to the top and right, the scaled loop shift (symbols and solid curves) and the loop shift expected from the unidirectional anisotropy (dotted curve) are plotted as a function of temperature. The arrows to the left of the $y$-axis give the loop shift calculated at $T = 0$ in the quasi-static limit.

FIG. 8. Coercivity, rotatable anisotropy, and rotational hysteresis. For different parameter values given to the top and right, the scaled coercivity (symbols and solid curves, the scaled rotatable anisotropy (dotted curve), and the scaled rotational hysteresis (dashed curve) are plotted as a function of temperature. The arrows to the left of the $y$-axis give the coercivity calculated at $T = 0$ in the quasi-static limit.

FIG. 9. Loop shift and coercivity. The scaled loop shift, $h_{\rm s}$ and coercivity $h_{\rm c}$ as a function of temperature are calculated for two different values of $s$, Eq. (4). The arrows to the left of the $y$-axis give the values calculated at $T = 0$ in the quasi-static limit.

FIG. 10. Coercivity as a function of thickness. Using the parameter values in Eq. (11) and the value of the antiferromagnetic domain wall energy $\sigma_0$=1.0 $\mathrm{mJ/m^2}$, the results from Fig. 9 are converted into the coercive field as a function of the thickness of the ferromagnetic film for several temperatures. Changing the value of the antiferromagnetic domain wall energy simply translates the curves horizontally.

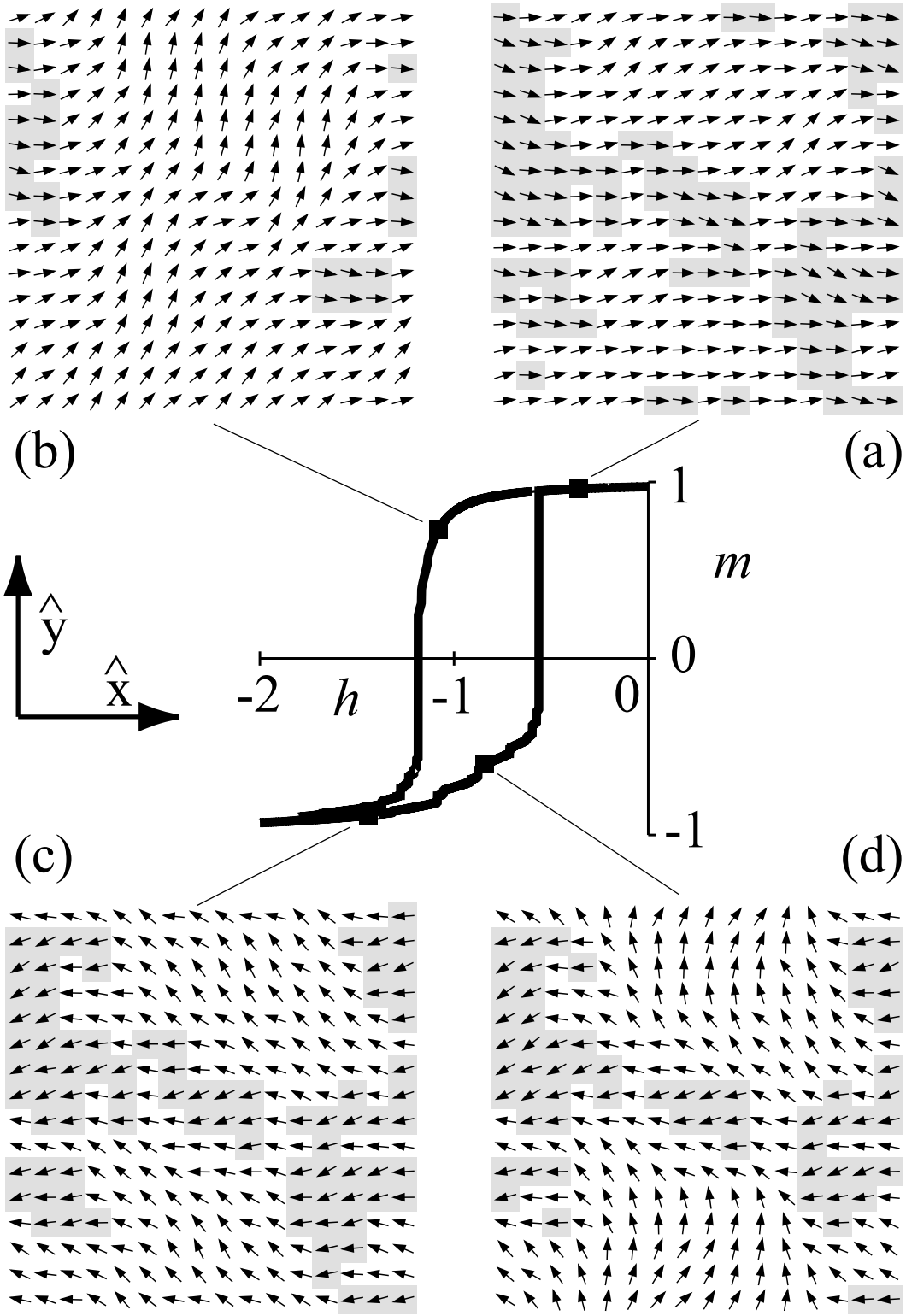


FIGURE 1

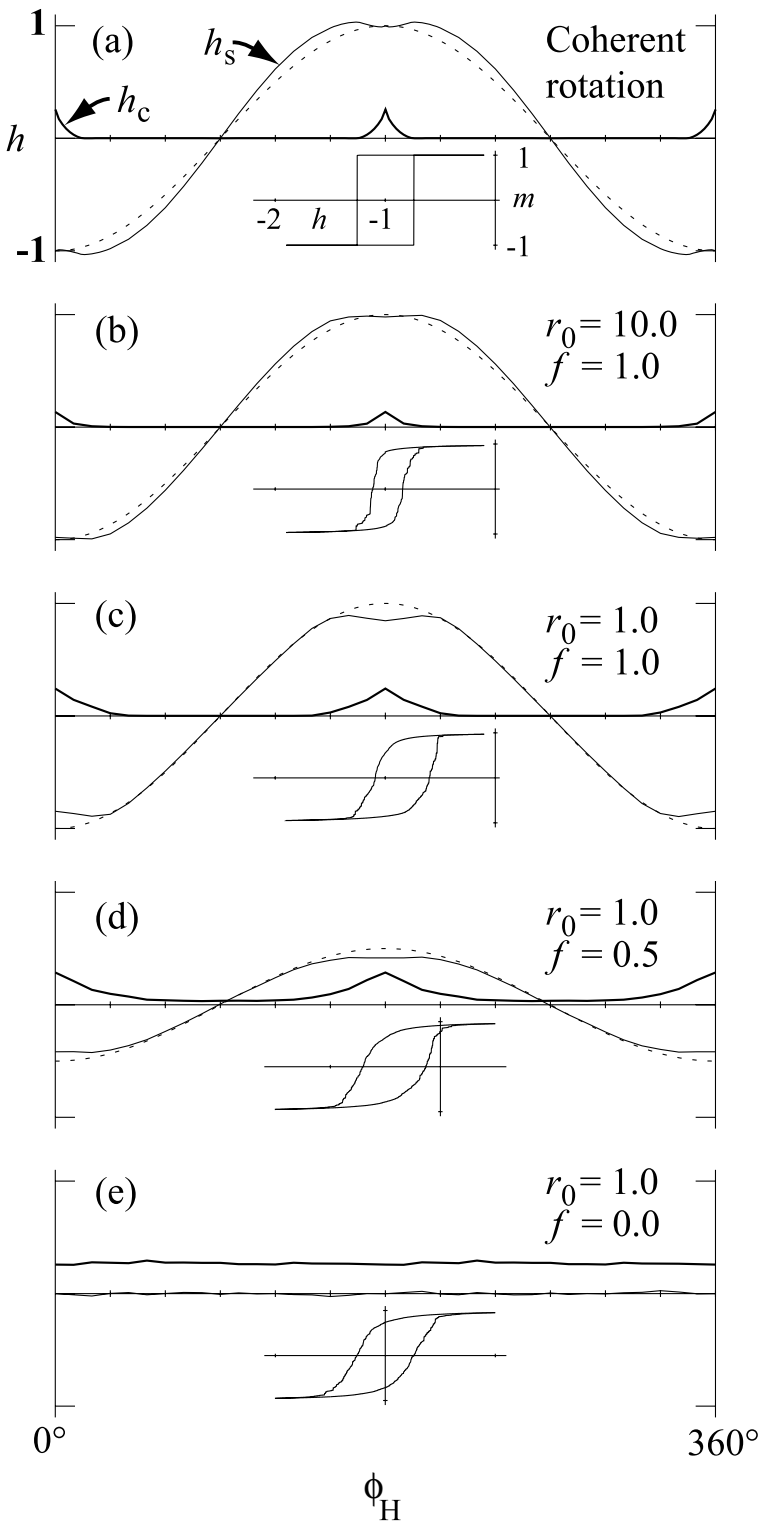
1
(a)
$h_s$
$h_c$
Coherent
rotation
$h$
-1
1
$m$
-2
$h$
-1
-1
(b)
$r_0$= 10.0
$f$ = 1.0
(c)
$r_0$= 1.0
$f$ = 1.0
(d)
$r_0$= 1.0
$f$ = 0.5
(e)
$r_0$= 1.0
$f$ = 0.0
0°
360°
$\phi_H$

FIGURE 2

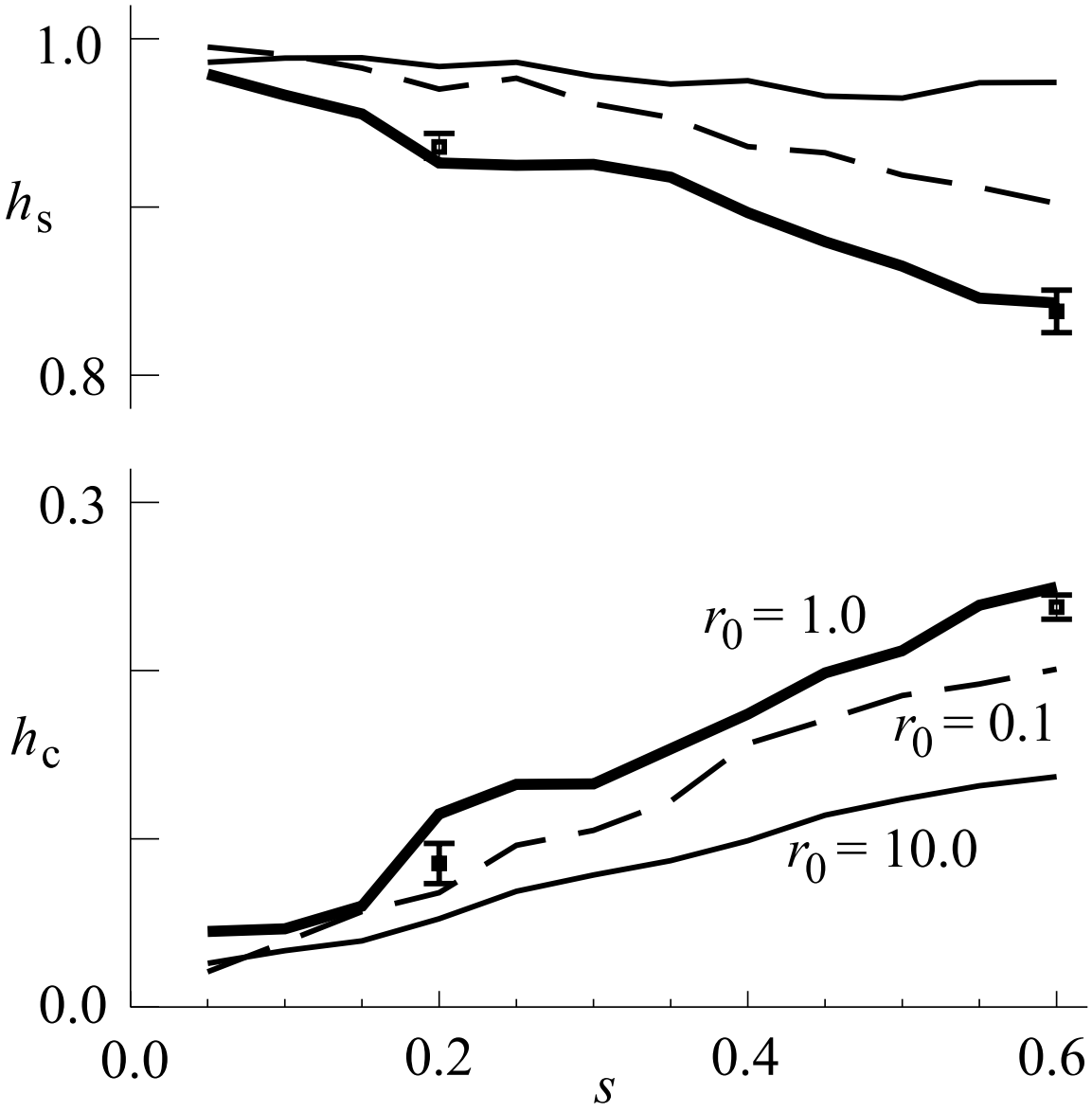


FIGURE 3

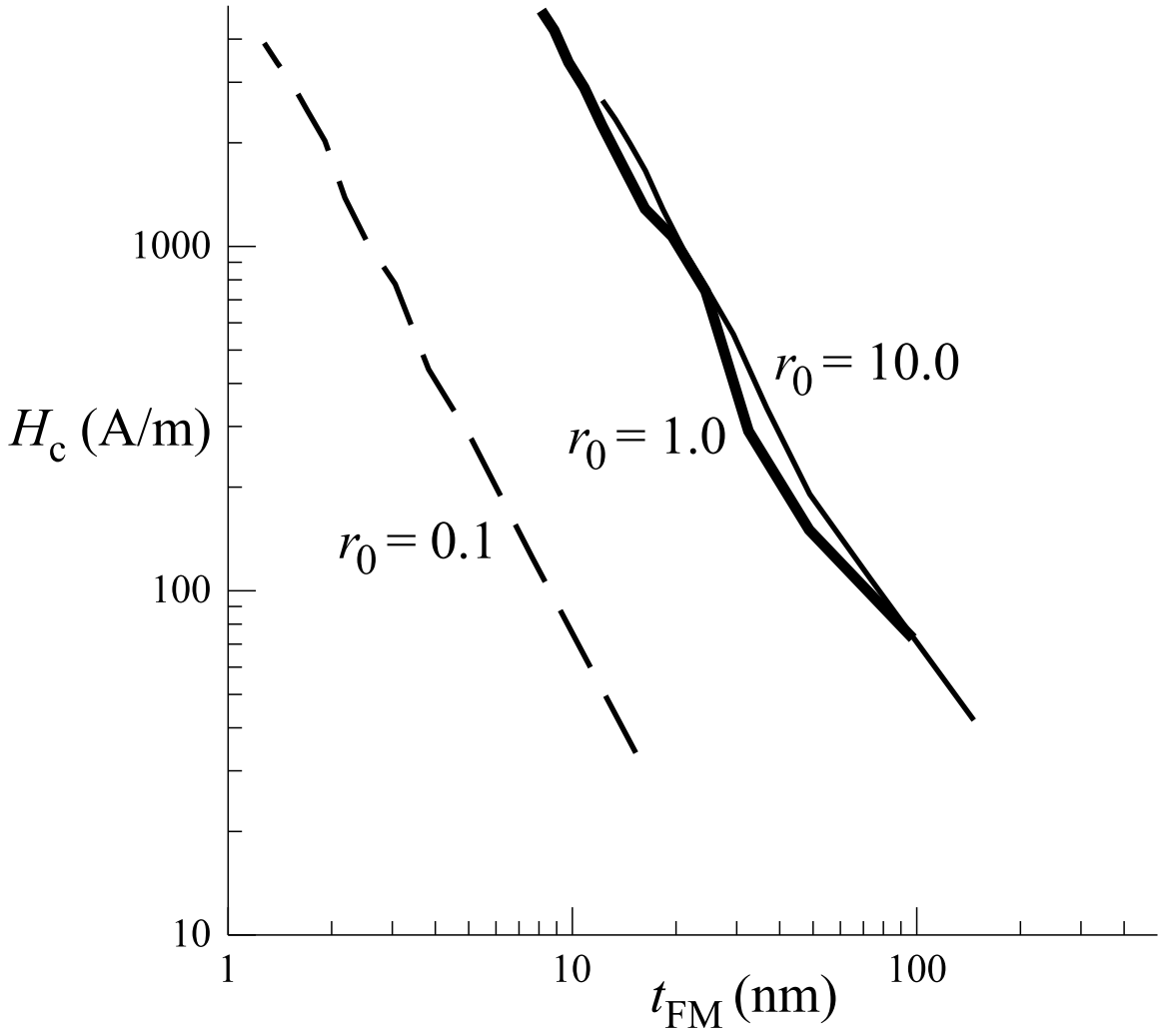


FIGURE 4

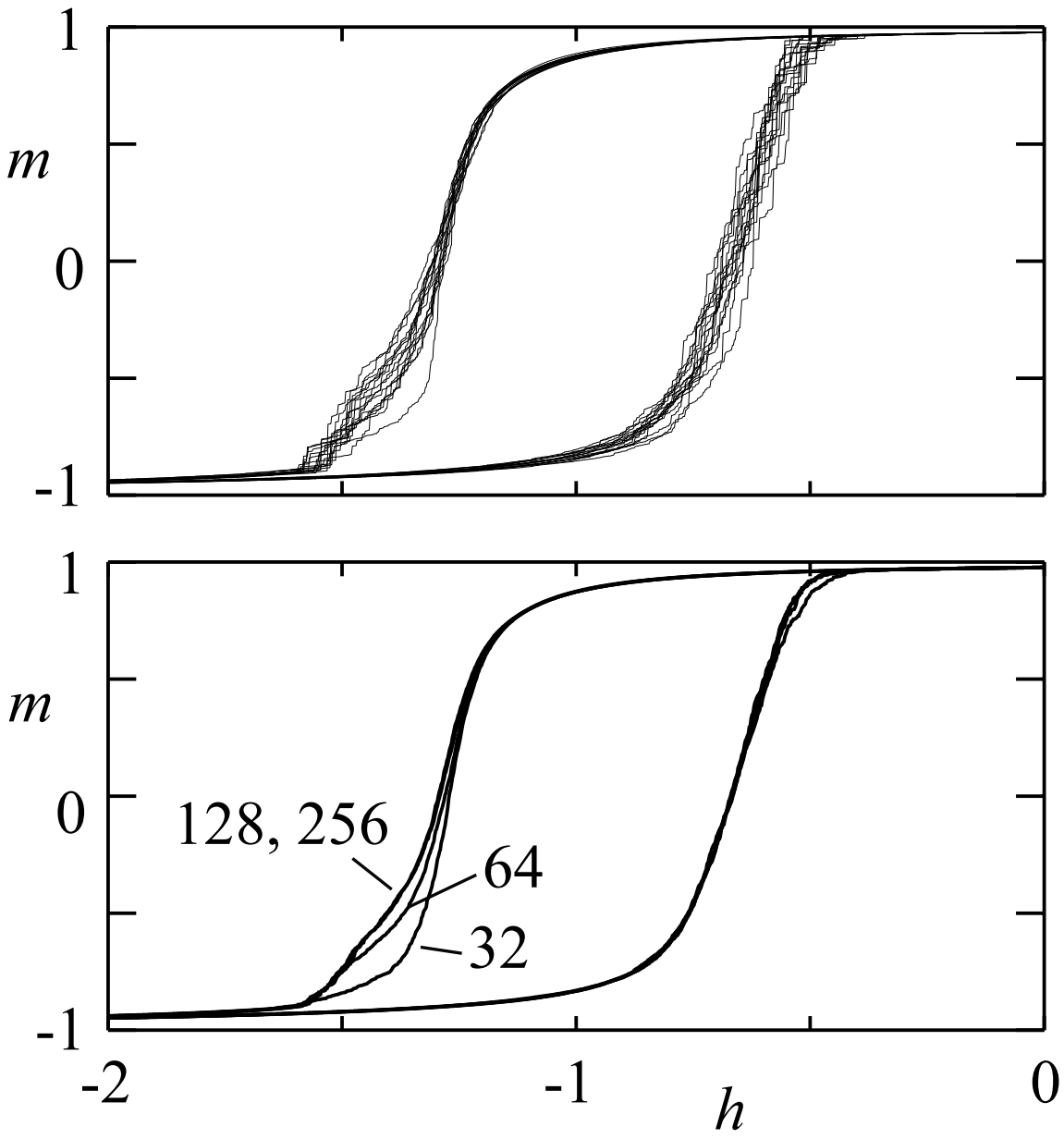


FIGURE 5

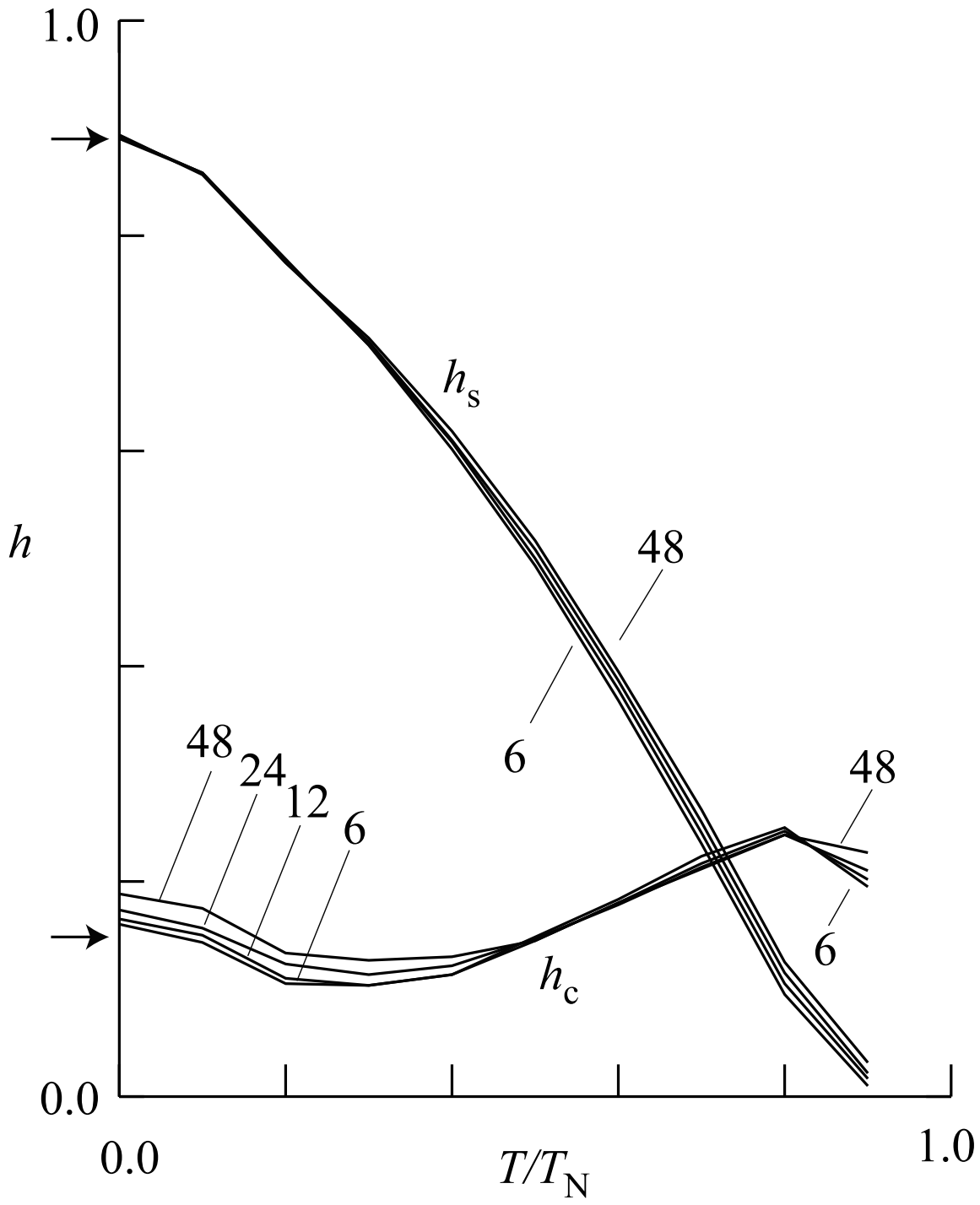


FIGURE 6

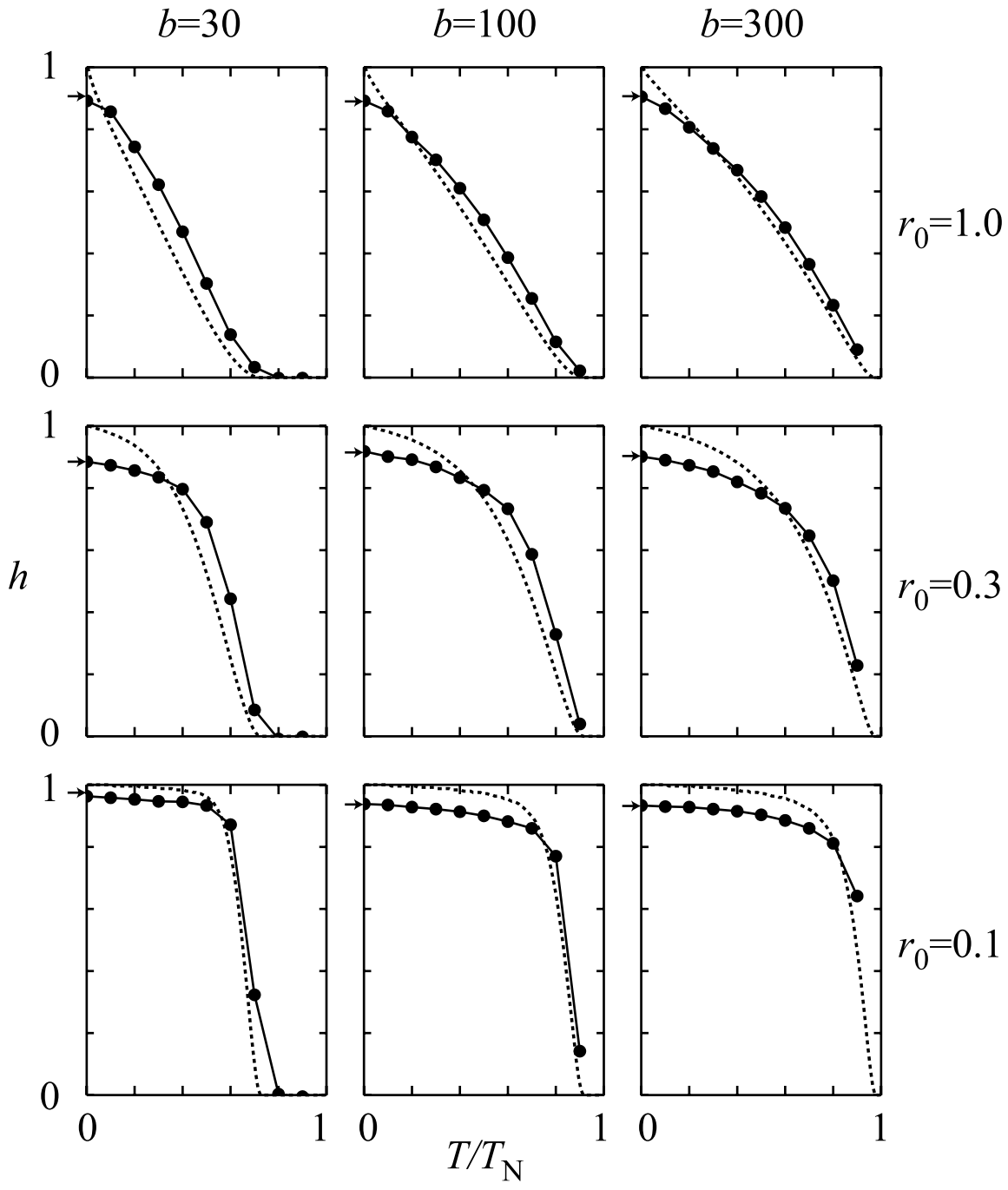


FIGURE 7

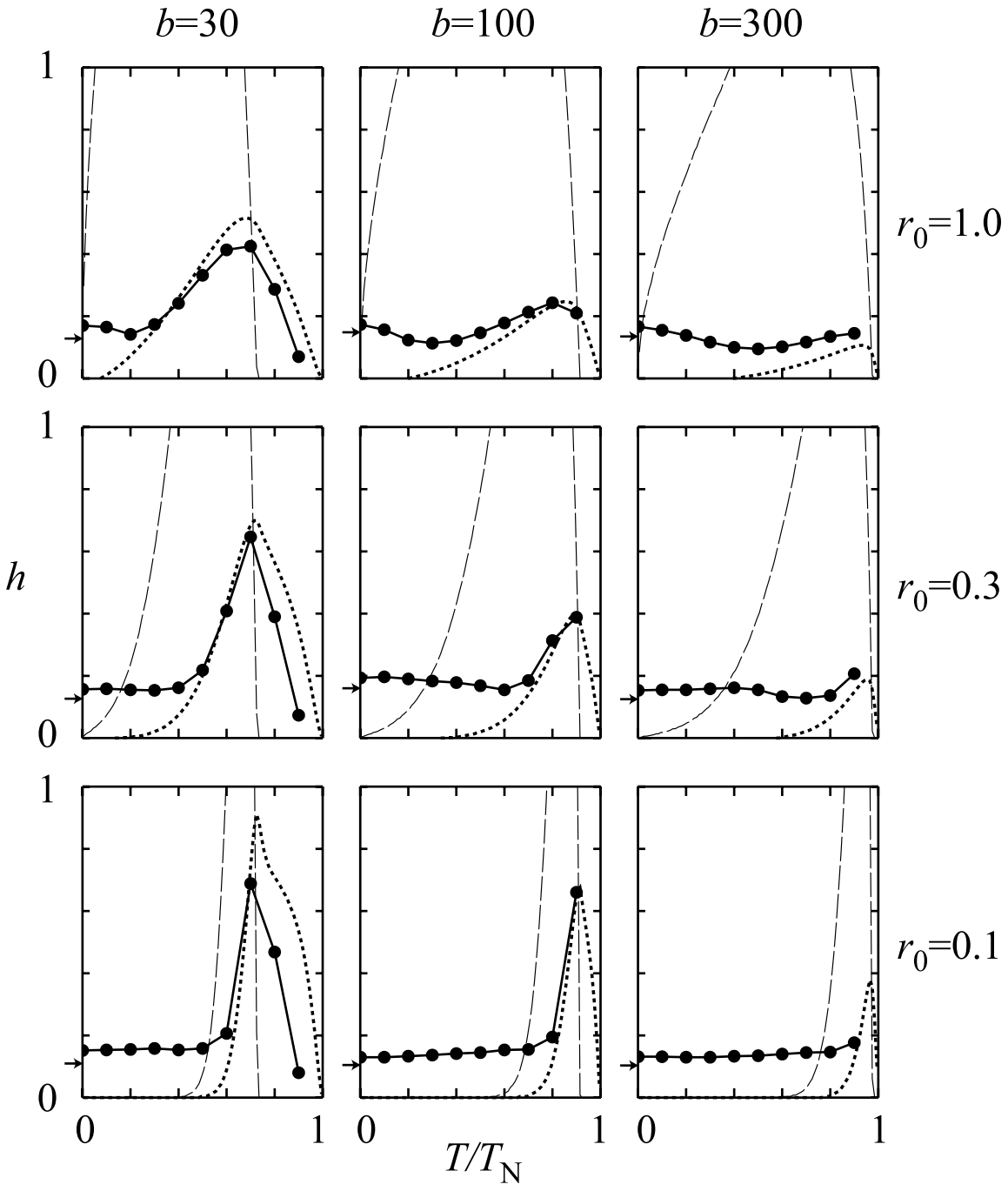


FIGURE 8

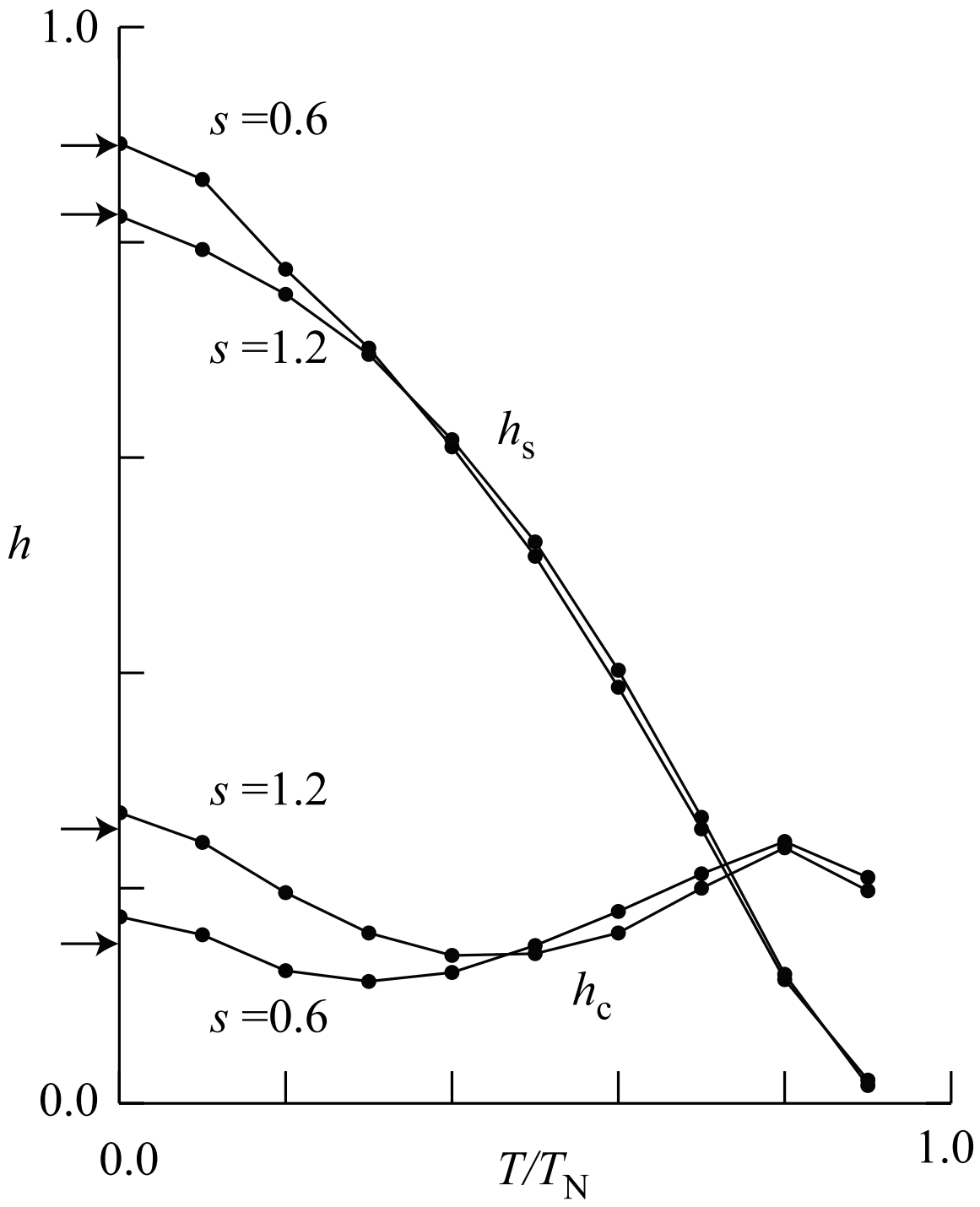


FIGURE 9

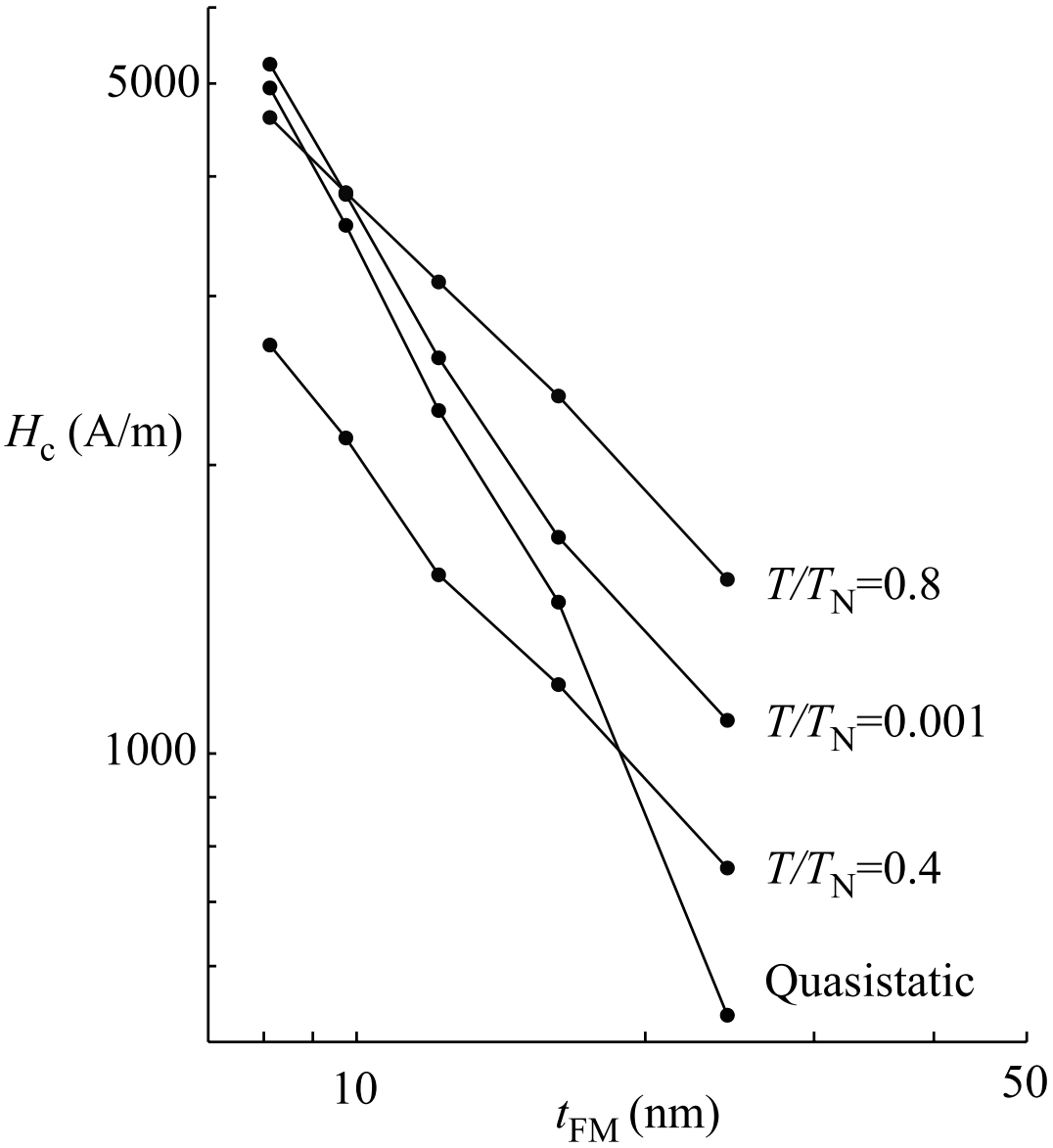


FIGURE 10